PAPER • OPEN ACCESS

Thermally induced all-optical ferromagnetic resonance in thin YIG films

To cite this article: Eva Schmoranzerová *et al* 2023 *New J. Phys.* **25** 033016

IOP Publishing New J. Phys. 25 (2023) 033016 https://doi.org/10.1088/1367-2630/acc203

New Journal of Physics
The open access journal at the forefront of physics

Deutsche Physikalische Gesellschaft DPG
IOP Institute of Physics

Published in partnership with: Deutsche Physikalische Gesellschaft and the Institute of Physics

OPEN ACCESS

RECEIVED
25 October 2022

REVISED
16 February 2023

ACCEPTED FOR PUBLICATION
7 March 2023

PUBLISHED
20 March 2023

PAPER

Thermally induced all-optical ferromagnetic resonance in thin YIG films

Eva Schmoranzerová[1,*], Jozef Kimák[1], Richard Schlitz[2], Sebastian T B Goennenwein[2,3], Dominik Kriegner[2,4], Helena Reichlová[2,4], Zbyněk Šobáň[4], Gerhard Jakob[5], Er-Jia Guo[5], Mathias Kläui[5], Markus Münzenberg[6], Petr Němec[1] and Tomáš Ostatnický[1]

[1] Faculty of Mathematics and Physics, Charles University, Prague, Czech Republic
[2] Department of Physics, Technical University Dresden, Dresden, Germany
[3] Department of Physics, University of Konstanz, Konstanz, Germany
[4] Institute of Physics, Academy of Sciences Czech Republic v.v.i, Prague, Czech Republic
[5] Institute of Physics, Johannes Gutenberg University, Mainz, Germany
[6] Institute of Physics, Ernst-Moritz-Arndt University, Greifswald, Germany
[*] Author to whom any correspondence should be addressed.

E-mail: eva.schm@karlov.mff.cuni.cz

Keywords: term, term, term

Supplementary material for this article is available online

Abstract

All-optical ferromagnetic resonance (AO-FMR) is a powerful tool for the local detection of micromagnetic parameters, such as magnetic anisotropy, Gilbert damping or spin stiffness. In this work we demonstrate that the AO-FMR method can be used in thin films of yttrium iron garnet (YIG) if a metallic capping layer (Au, Pt) is deposited on top of the film. Magnetization precession is triggered by heating of the metallic layer with femtosecond laser pulses. The heat pulse modifies the magneto-crystalline anisotropy of the YIG film and shifts the quasi-equilibrium orientation of the magnetization, which results in precessional magnetization dynamics. The laser-induced magnetization precession corresponds to a uniform (Kittel) magnon mode, with the precession frequency determined by the magnetic anisotropy of the material as well as the external magnetic field, and the damping time set by a Gilbert damping parameter. The AO-FMR method thus enables measuring local magnetic properties, with a resolution given by the laser spot size.

1. Introduction

Among the many mechanisms that can trigger magnetization dynamics in solids, only the interaction with ultrashort laser pulses allows to coherently access the very fastest processes at femtosecond time-scales [1–4]. Various ways the laser pulses can interact with magnetic materials have been reported in the past years, including ultrafast spin-transfer [5, 6], ultrafast demagnetization [7–12], optical spin transfer and spin orbit torques [13–15] or laser-induced phase transitions [16, 17]. All these effects set the magnetic system out of equilibrium, and can induce a precession of the magnetization. The laser-induced magnetization precession is an important research field of its own, as it enables investigating the various excitation mechanisms and their symmetries [2]. But it also represents an all-optical analogy of the microwave-based ferromagnetic resonance (MW-FMR), providing valuable information about the fundamental parameters of magnetic materials such as their spin stiffness, magnetic anisotropy or Gilbert damping [18]. The 'all-optical FMR' (AO-FMR) is a local and non-invasive method, with spatial resolution governed by the laser spot size which can be focused down to a few micrometres, a property particularly favourable for investigating model spintronic devices.

Magnetization precession has already been described in various classes of materials including ferromagnetic metals [19–21], semiconductors [18, 22], or even in materials with a more complex spin structure such as non-collinear antiferromagnets [23]. Ferrimagnetic insulators, with yttrium iron garnet (YIG, $Y_3Fe_5O1_2$) as the prime representative [24], are of particular importance for spintronic applications

owing to their high spin pumping efficiency [25] and the lowest known Gilbert damping [26]. However, inducing magnetization dynamics in ferrimagnetic garnets optically is quite challenging, as it requires large photon energies of pump pulses (the bandgap of YIG is $E_g \approx 2.8$ eV) [27] while the most common ultrafast laser systems usually generate light in the near-infrared spectral region. In principle, it is possible to reach the required spectral range by a frequency doubling of the laser output yet the resulting pulse energy is typically too low to be used as 'pump' pulses. Therefore, only non-thermal triggers for the magnetization precession have been exploited in YIG, such as inverse Faraday [28, 29] and Cotton–Mouton [30] effects, or photoinduced magnetic anisotropy [31, 32]. For these phenomena to occur, large laser fluences of tens of mJ cm^{-2} are required [33]. In contrast, tens of μJ cm^{-2} are sufficient for the thermal excitation of magnetization precession in most of the magnetic systems [22, 23, 31]. This low fluence regime provides distinct advantages in determination of quasi-equilibrium material parameters, unaffected by the strong laser pulses, as discusses e.g. in [18–20]. The thermal excitation of magnetization has naturally been attempted in magnetic garnets as well. However, it required complex artificial engineering of a magnetic anisotropy of the garnet via inclusion of the bismuth dopants [31], a method that is not suitable in spintronic and magnonic devices and is viable only in a small subset of garnet materials.

In this paper, we show that upon capping a pure YIG film with a thin metallic layer, magnetization precession can be induced thermally by femtosecond laser pulses. The laser pulses locally heat the system, which sets the magnetization out of equilibrium due to a temperature dependence of its magnetocrystalline anisotropy and/or demagnetization. Consequently, a Kittel FMR mode (homogeneous precession) is generated, with a precession frequency corresponding to the quasi-equilibrium magnetic anisotropy of the thin YIG film [34]. Using the AO-FMR method we revealed an increase of the Kittel mode damping at cryogenic temperatures, which is in agreement with the previous microwave FMR experiments [35, 36]. Not only does this demonstrate the AO-FMR technique as a sensitive, local tool for the evaluation of the micromagnetic parameters of YIG, it also reveals the potential of AO-FMR in studying other spin-related phenomena in thin YIG films and heterostructures, such as spin pumping [37, 38] or ultrafast spin-Seebeck effect [5, 6] directly in the time domain. Furthermore, the universal nature of this method makes it applicable to many wide-gap insulator systems that are not accessible by conventional optical pump-probe experiments.

2. Experimental method

Our experiments were performed on a 50 nm thick layer of stoichiometric $Y_3Fe_5O_{12}$ grown by pulsed-laser deposition on a gadolinium–gallium-garnet (GGG) (111)-oriented substrate. One part of the film was covered by 8 nm of Au capping layer (further referred as YIG/Au), another one by Pt capping (YIG/Pt). Both the metallic layers were prepared by ion-beam sputtering. The remaining YIG layer was left uncapped as a reference. X-ray diffraction confirmed good crystallinity of the YIG film with a low level of growth-induced strain, as described in detail in [39]. The magnetic properties were further characterized using SQUID magnetometry and conventional MW-FMR, showing the film plane is an easy plane of magnetization (see figures S1 and S2 in supplementary material). The saturation magnetization of the YIG layer $\mu_0 M_s \approx 180$ mT at cryogenic temperatures ($T = 20$ K) corresponds well to the results published on qualitatively similar samples [40], again confirming quality of the film. In addition, the magnetic anisotropy of the system was established from an independent magneto-optical experiment [34]. The corresponding anisotropy constants for cubic anisotropy of the first and second order are $K_{c1} = -4680$ J m^{-3} and $K_{c2} = -223$ J m^{-3}, while the uniaxial out-of-plane anisotropy K_u is vanishingly small.

Laser-induced magnetization dynamics was studied in a time-resolved magneto-optical experiment in transmission geometry, as schematically shown in figure 1(a). The output of a Ti:Sapphire oscillator (MaiTai, Spectra Physics) generating 200 fs laser pulses with repetition rate of 82 MHz was divided into a strong pump beam and significantly weaker probe beam. Pump fluence was tuned between 70 and 280 μJ cm^{-2}, while the probe beam was typically 20-times weaker. Both beams were focused on a 30 μm spot on the sample, placed in a closed-cycle cryostat (ARS Systems) and kept at cryogenic temperatures, usually at $T = 20$ K. An external magnetic field of up to 550 mT, generated by a two-pole electromagnet, was applied in y direction (see figure 1). The wavelength of the pump pulses (800 nm) was set well below the absorption edge of the YIG layer, as indicated in the transmission spectrum of the sample in figure 1(b). The wavelength of the probe pulses (400 nm) was matched to an interval of a strong magneto-optical response of bulk YIG (see inset in figure 1(b) and [41]).

The time-resolved magnetooptical (TRMO) signal was measured as a function of the time delay Δt between pump and probe pulses. The corresponding pump-induced rotation of the polarization plane of the probe beam $\Delta\beta$ was detected using an optical bridge technique combined with a phase-sensitive lock-in detection (see appendix B in [42]). Simultaneously, the time-resolved modification of the sample transmission (TRT) $\Delta T/T_0$ was recorded, where T_0 stands for the equilibrium transmittance.

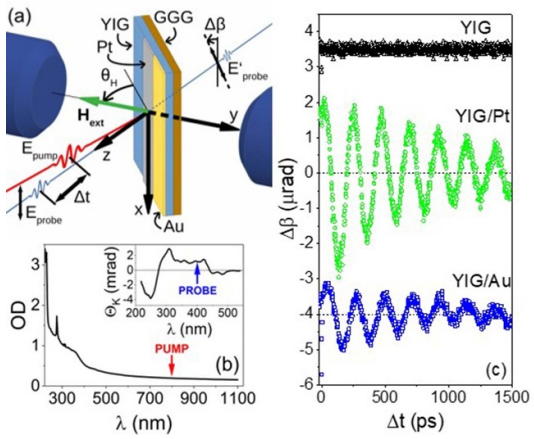

Figure 1. (a) Schematic illustration of the pump&probe experimental setup, where E_{probe} is the probe beam linear polarization orientation which is rotated in the sample by an angle $\Delta\beta$ to the orientation E'_{probe}. An external magnetic field H_{ext} (depicted by the green arrow) is applied at an angle θ_H. (b) Absorption spectrum of the studied YIG sample, where OD stands for the optical density defined as minus the decadic logarithm of the sample transmittance. The red arrow indicates the wavelength of the pump beam $\lambda_{\mathrm{PUMP}} = 800$ nm. Inset: Spectrum of Kerr rotation Θ_{K} of a bulk YIG crystal [41]. The blue arrow shows the wavelength of the probe beam $\lambda_{\mathrm{PROBE}} = 400$ nm. (c) Typical time-resolved magneto-optical signals of a plain 50 nm YIG film (black dots), YIG /Pt (green dots) and YIG/Au bilayers (blue dots) at 20 K and $\mu_0 H_{\mathrm{ext}} = 100$ mT, applied at an angle $\theta_H = 40°$.

3. Laser-induced magnetization precession and its origin

An example of TRMO signals of uncapped YIG and two YIG/metal heterostructures is shown in figure 1(c). Clearly, in the presence of the metallic capping layer an oscillatory TRMO trace is observed, whose amplitude depends on the type of the capping metal. Frequency and damping of the oscillations, on the other hand, remain virtually unaffected by the type of the capping layer. In the uncapped YIG sample, in contrast, we do not detect any oscillatory behaviour.

The TRMO signals can be phenomenologically described by a damped harmonic function, superimposed on a slowly-varying background [22]:

$$\Delta\beta(\Delta t) = A\cos(2\pi f\Delta t + \varphi)\exp(-\Delta t/\tau_{\mathrm{D}}) + B\exp(-\Delta t/\tau_{\mathrm{R}}) \tag{1}$$

where A is the amplitude of precession, f its frequency, φ the phase and τ_{D} the damping time. The background can be approximated by an exponential decay function with amplitude B and relaxation time τ_{R}. An example of the resulting fit is shown as a red line in figure 2(a), decomposed for clarity to the oscillatory part (blue line) and the time-dependent background (green line).

In order to confirm magnetic origin of the TRMO traces, we varied the external magnetic field H_{ext} and extracted the particular precession parameters by fitting the detected signals by equation (1). As depicted in figure 2(b), the dependence of the precession frequency on the applied field obtained from the TRMO experiment is in excellent agreement with the solution of the Landau–Lifshitz–Gilbert (LLG) equation, using the free energy of a [111] oriented cubic crystal (see supplementary material, section B, equation (S5) and [34]). This correspondence with the LLG model proves that our oscillatory signals reflect indeed the precession of magnetization in a uniform (Kittel) mode in YIG. We stress that the precession frequency is inherent to the YIG layer and does not depend on the type of the capping layer, as apparent from figure 2(b).

We can further confirm the uniform Kittel mode by comparing frequency f of the oscillations from the TRMO experiment with the frequency of resonance modes observed in a conventional, MW-FMR. TRMO signals in YIG/Au sample were measured in a range of polar field angles θ_H, and modelled by LLG equation with the same parameters that were used in figure 2(a). The output of the modelled $f(\theta_H)$ dependency is presented in figure 2(c), together with precession frequencies obtained from TRMO and MW-FMR experiments. Note that the MW-FMR was performed only in the in-plane ($\theta_H = 0°$) and out-of-plane ($\theta_H = 90°$) geometry of the external magnetic field. Clearly, the MW-FMR data fit well to the overall trend given by LLG equation, which indicates that the TRMO method indeed provides an all-optical analogy to the FMR technique [43].

So far, we have focused only on the character of the magnetization precession. The question remains as to the mechanism that triggers the magnetization dynamics. The pump pulses can affect thin magnetic layers by various processes. A torque exerted on magnetization can be related to spin transfer via spin current [13, 14], or can be caused by thermal modification of magnetic properties [18, 20–22]. In principle, also the

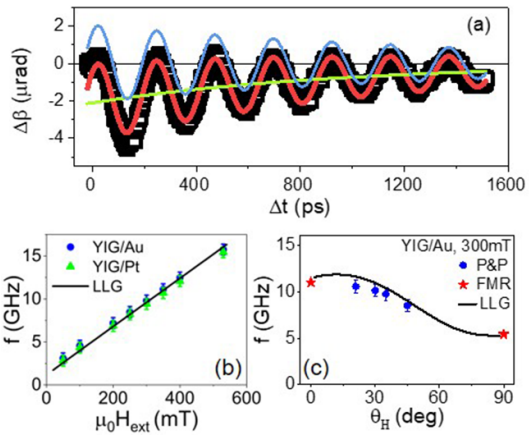

Figure 2. (a) Example of fit of time-resolved magneto-optical signals. Black dots correspond to the as-measured signals, red line indicate fit by equation (1). The fitted curve contains two independent components, the damped oscillatory signal (blue line) and the slowly-varying background (green line). The data were taken at external field of $\mu_0 H_{ext} = 100$ mT, $T = 20$ K and $I = 140$ μJ cm^{-2}, $\theta_H = 40°$. (b) Frequency f of magnetization precession as a function of magnetic field applied at an angle $\theta_H = 40°$, for YIG/Pt (blue dots) and YIG/Au (green triangles) at $T = 20$ K and $I = 150$ μJ cm^{-2}. The line is calculated from the LLG equation (equation (S3)) with the free energy given by (equation (S5)). (c) Field-angle dependence of f obtained from the pump-probe (P&P) experiment in YIG/Au sample for $\mu_0 H_{ext} = 300$ mT (blue dots), compared to a model by LLG model (line) and to frequencies measured by MW-FMR (red stars) [43].

spin-Seebeck effect [5, 6] can be a source of the torque. Each of these phenomena shows certain fingerprints, yet the most dominant is their relevant timescale, which limits how fast the dynamics can be triggered and leads to a characteristic phase of the magnetization precession (see supplementary note 1 in [44]). However, a straightforward analysis of the phase is only possible if the polar Kerr effect dominates magneto-optical response of the studied system. If more magneto-optical (MO) effects are intermixed in the signal, the initial phase is given also by the polarization angle of the linearly polarized light. This is the case of our sample, where linear and quadratic MO effects of similar strength are present (see [34]), resulting in a non-trivial polarization dependence of the initial precession phase, as shown in figure 3(a). Such behaviour prevents analysing the phase as a simple marker of the underlying physical mechanism. Yet there are still some common features in the signals in figure 3(a), independent of the light polarization. The most remarkable one is the slow onset of the precession signal. To highlight this onset, in figures 3(a) and (b) we show the measured TRMO traces together with their fits by equation (1), representing our model of magnetization precession. Our model describes the precession very well on the longer timescales (figure 3(a)) but fails in the first ≈20 ps after the excitation (figure 3(b)). In order to understand this behaviour, we compare the magnetization dynamics detected by TR-MOKE with that of TRT, which reveals carrier as well as the heat transfer dynamics [8, 18, 42] in the studied heterostructure. Clearly, there is a significant shift in the signal onsets: In TR-MOKE, a rather large signal is detected immediately after impact of the pump pulse, but it takes ≈10 ps before it can be properly described by our magnetization precession model. Strikingly, equal amount of time is needed for TRT to reach its maximum value, see figure 3(b). There is also a significant difference in the initial stage of TRT both in amplitude and shape, depending on the type of the metal capping figure 3(c). After ≈ 20 ps, a slowly varying signal appears in TRT that is independent of the metallic layer figure 3(d). The capping thus seems to play a role only in the first few picoseconds after the excitation, which corresponds to the thermalization of the metal layer [42]. After that, the heat is distributed to the whole heterostructure. On a timescales of nanoseconds (figure 3(d)), the TRT is dominated by the YIG layer and reflects the slow heat flow from YIG to the GGG substrate [42]. The slowly-varying background modulating the oscillatory TRMO signals see figure 2(a) is relaxed on ns timescales as well, and is very likely associated with the same cool-down process of the YIG layer to the substrate. Finally, note that no oscillatory component indicating the laser-induced phonon modes is observed in the TRT signals that could possibly trigger a magnetization dynamics in the YIG layer.

All the experimental observations described in the previous paragraph strongly indicate a thermal origin of the magnetization precession. The optical spin torques take place on ultrashort timescales below 1 ps (see, e.g. figure 2 in [14] and figure 1(d) in [15]), and we can exclude them by the relatively long ≈ 20 ps onset of the precession in our signals. On the other hand, the thermal effects are known to be significantly slower [15, 44] and they share one particular finger print—the torque induced by thermal modification of magnetic properties is typically strongly dependent on the applied external magnetic field (see the discussion in supplementary note 1 in [44]). In figure 4(a) we show the amplitude A of the oscillatory part of the TRMO

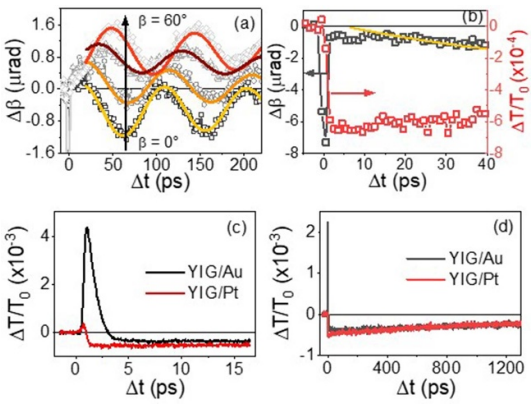

Figure 3. (a) Time-resolved MO signals (points), detected for different probe polarization orientations β and fitted by equation (1) ($\beta = 0°$—yellow line, 30°—orange, 45°—red, and 60°—dark red), yielding precession initial phases φ of $-60°$,$-75°$,$-133°$, and $-6°$, respectively. (b) Time-resolved transient transmission $\Delta T/T_0$ (red points) and magneto-optical signal $\Delta\beta$ (black points), fitted by equation (1) (line) in the YIG/Au sample for $\beta = 0°$. (c) and (d) Comparison of time-resolved transient transmission traces in YIG/Pt and YIG/Au structures, shown at ultrashort (c) and longer (d) time delays between pump and probe pulses Δt. $T = 20$ K, $I = 150$ μJ cm^{-2}, $\mu_0 H_{ext} = 300$ mT.

signal as a function of the external magnetic field H_{ext}. The precession is apparently vanishing close to $\mu_0 H_{ext} = 0$ mT which is consistent with the expected thermally-induced torque. It peaks around $\mu_0 H_{ext} \approx 100$ mT, where the effective internal fields (i.e. demagnetization or anisotropy fields) of the YIG layer equalize with H_{ext}, making the magnetization more susceptible to external stimuli [7–10]. In addition, both in YIG/Au and YIG/Pt, the $A(H_{ext})$ dependence maintains the same character. Such behaviour is not expected for the torque resulting from the ultrafast spin-Seebeck effect which would have a character of spin-torque; i.e. it would depend on the type of the metal capping. Therefore, we interpret the heat-induced modification of the magnetic properties of the garnet as the main mechanism triggering the magnetization precession in our YIG/metal bilayer. The heat generated in the metallic layer by the absorption of the laser pulse propagates towards the YIG layer and modifies its properties by two distinct mechanisms: demagnetization and/or change of the magnetic anisotropy. To separate these two effects, in figure 4(b) we plot a temperature dependence of the saturation magnetization $M_s(T)$, as obtained on a very similar YIG layer in [45]. The inset of figure 4(b) shows the amplitude of the oscillatory TRMO signal measured in our YIG/Pt structure as a function of the ambient temperature $A(T)$. It is reasonable to expect that the magneto-optical coupling is not strongly temperature dependent in the studied range (see [34]). The amplitude of the TRMO signal thus corresponds directly to the precession amplitude of the magnetization vector. By comparing the $M_s(T)$ and $A(T)$ dependencies in figure 4(b) we clearly see that, even assuming the most extreme laser-induced increase in quasi-equilibrium (nanosecond timescale) temperature $\Delta T \approx 80$ K (see figure 4(d) and the related discussion), the laser-induced variation of M_s would be less than 5%, while the precession amplitude A changes by more than 50% between 20 and 50 K. Consequently, the laser-induced heating would not modify the saturation magnetization enough to account for the observed drop in the magnetization precession amplitude, and thus it is less likely to be the main mechanism behind the magnetization precession.

Overall, the thermal modification of magnetocrystalline anisotropy, occurring at the timescale of the first 10 ps, remains as the most plausible effect responsible for exerting a torque on magnetization. In figure 4(c) we plot the cubic magnetocrystalline anisotropy energy K_{c1} as a function of the sample temperature (obtained from [34, 45]), together with the precession frequency f from our TRMO experiment. In order to establish a mutual connection between these two quantities, we calculated the frequency f as a function of anisotropy constant K_{c1} directly from the LLG equation. This calculation, presented in the inset of figure 4(c) revealed proportionality between f and K_{c1} in our narrow temperature window, which allows for the direct comparison of $K_{c1}(T)$ and $f(T)$ dependencies in figure 4(c). Clearly, both K_{c1} and f vary strongly with temperature. $K_c(T)$ and $f(T)$ show a similar trend which leads us to conclusion that the laser-heat-induced modification of K_{c1} is indeed the mechanism triggering the magnetization precession. Changing the anisotropy constant K_{c1} shifts the quasi-equilibrium position of the magnetic easy axis, which exerts a torque on magnetization, in a mechanism similar to that observed in ferromagnetic semiconductors [18].

The linear dependence between K_c and f allows us also to estimate the pump-induced increase ΔT in the quasi-equilibrium temperature of the sample (see, e.g. [18]). The corresponding values of ΔT are plotted in figure 4(d) together with the corresponding precession frequencies. As expected, a higher laser fluence leads

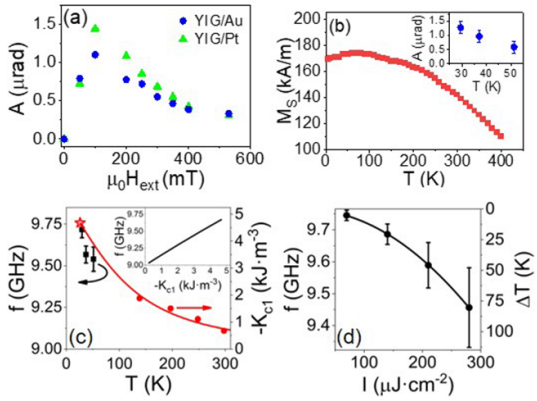

Figure 4. Origin of the magnetization precession in YIG film (a) precession amplitude A as a function of external magnetic field H_{ext} (dots) in YIG/Pt and YIG/Au. (b) Temperature dependence of saturation magnetization M_s obtained from [45]. Inset: temperature dependence of the precession amplitude A measured for $\mu_0 H_{ext} = 300$ mT. (c) Temperature dependence of precession frequency f in the YIG/Au sample (black points), where $\mu_0 H_{ext} = 300$ mT was applied at $\theta_H = 40°$. The temperature dependence of cubic anisotropy constant K_{c1} was obtained from [34] (red dots) and [45] (red star at $T = 20$ K); $I = 15$ μJ cm^{-2}. The data were fitted by an inverse polynomial dependence $K_{C1}(T) = \frac{1}{(a+bT+cT^2)}$, with parameters: $a = 0.18$ m^2 kJ^{-1}; $b = 9 \times 10^{-4}$ m^2 kJ^{-1}.K; $c = 9 \times 10^{-6}$m^2 kJ^{-1}.K^2. Note that the fitting function is phenomenological only. Inset: dependence $f(K_{c1})$ obtained from the LLG equation. (d) f as a function of pump pulse fluence I, from which the increase of sample temperature ΔT for the used pump fluences was evaluated using the $f(T)$ dependence; $\theta_H = 40°$, $T = 20$ K.

to a more pronounced heating, which results in a decrease of f. Note that for the highest intensity of 300 μJ cm^{-2}, the sample temperature can increase by almost 80 K. However, the level of heating and the particular heat propagation dynamics depends strongly on the metallic capping, as discussed in the next section.

4. Effect of metallic capping on heat propagation

In the previous section, we have shown that the measured magnetization dynamics reflect the properties of the YIG film, yet the main source of the laser-induced heating is the metallic layer. Let us now focus on the capping metal, and the role it plays in the trigger efficiency for the laser-induced magnetization precession. In figure 5(a) we plot the amplitude A of the oscillatory signal in the YIG/Pt and YIG/Au as a function of the laser intensity I. Clearly, the precession amplitude and its intensity dependence is significantly larger in YIG/Pt. Furthermore, precession damping is weaker in YIG/Pt than in YIG/Au, as apparent from figure 5(b) where an effective Gilbert damping parameter α_{eff} is plotted as a function of H_{ext}. The effective damping parameter was obtained by fitting the TRMO data directly by LLG equation, as detailed in supplementary material, section B. Despite the relatively large fitting error, YIG/Pt shows systematically lower values of $\alpha_{Pt} \approx (0.020 \pm 0.003)$ than YIG/Au where $\alpha_{Au} \approx (0.025 \pm 0.003)$. Origin of the unusually high Gilbert damping shall be discussed in more detail below.

To understand these differences, we modelled the propagation of laser-induced heat in GGG/YIG/Pt and GGG/YIG/Au multilayers by using the heat equation (see supplementary material, section E). In figure 5(c), the calculated increase in temperature ΔT is shown as a function of time delay Δt after pump excitation for selected depths from the YIG surface. In figure 5(d), the same calculations are shown for variable depths and fixed Δt. The model clearly demonstrates that a significantly higher ΔT can be expected in the Pt-capped layer simply due to the stronger light absorption and smaller energy loss by reflection in this metal (see supplementary material, section E). This in turn leads to a higher amplitude of the laser-induced magnetization precession in YIG/Pt compared to the YIG/Au, as apparent in figure 5(a). According to our model, significant increase in temperature (tens of Kelvins) is generated in the first ten picoseconds after excitation. This fast heat dynamics agrees very well with the experimentally assessed dynamics of the sample reflectivity figure 3(c), again confirming the thermal trigger of the magnetization precession.

The precession frequency that we detect reflects the quasi-equilibrium state of the system, i.e. a regime not influenced by a presence of the pump pulse. Therefore, the temperature increase ΔT deduced from the TRMO signal can be compared with our model for large enough time delays after the excitation ($\Delta t \gg 20$ ps). Clearly, the values given by our model are a factor of ≈10 smaller (see figures 4(d) and 5(c) for comparison). This discrepancy results from the boundary conditions of our model that assumes an ideal heat transfer between all the sample layers, and between the sample and the cryostat sample holder. In the real experiment, the heat conduction is limited by heat insulation of the metal/YIG and YIG/GGG boundaries,

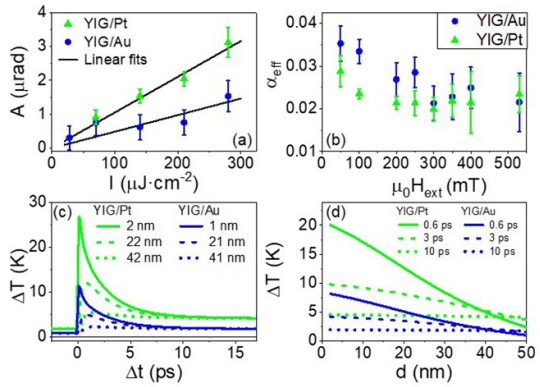

Figure 5. Comparison of magnetization precession in YIG/Pt and YIG/Au samples. (a) Precession amplitude A as a function of pump fluence I (dots) measured for $\mu_0 H_{ext} = 300$ mT and $T = 20$ K. The lines are the linear fits $\boldsymbol{A} = \boldsymbol{s}\cdot\boldsymbol{I}$ with $s_{Pt} = (1.05 \pm 0.09) \times 10^{-2}$ μrad.cm^2 μJ^{-1} in YIG/Pt and $s_{Au} = (0.5 \pm 0.1) \times 10^{-2}$ μrad.cm^2 μJ^{-1} in YIG/Au. In YIG/Pt, the as-measured data obtained for $\theta_H = 40°$ are shown. In the YIG/Au, the $A(I)$ dependence was originally measured for $\theta_H = 21°$ and recalculated to $\theta_H = 40°$ according to the angular dependence, as described in detail in supplementary material, section C. (b) Gilbert damping α_{eff} for H_{ext} applied at an angle $\theta_H = 40°$. The values of α_{eff} result from fitting the TRMO signals by LLG equation. (c) and (d) Increase in lattice temperature as a function of time delay between pump and probe pulses for selected depths from the sample surface (c) and as a function of depth for fixed time delays (d); $I = 140$ μJ cm^{-2}, $T_0 = 20$ K. The heat capacities and conductivities of layers are provided in the supplementary material, section 7.

and by a silver glue used to attach the sample to the cryostat coldfinger. We also have to consider that only equilibrium heat conductivity and capacity of bulk materials were available for the calculations. However, these parameters are known to differ significantly in layers with a thickness of only a few lattice constants [46, 47] can also affect the results of our model.

Results of the model in figure 5(d) further indicate formation of relatively large thermal gradients across the 50 nm YIG layer in the first few picoseconds after the excitation. These gradients could give rise to spin-related phenomena, such as spin-Seebeck effect [5, 6]. While no such effect could be clearly identified in our current experimental results (see section 3), the TRMO experiment is very well suited for an eventual detection of the spin-Seebeck induced torque.

The same laser-induced thermal gradients can also result in an increase in damping of the magnetization precession by an extrinsic term. As our effective Gilbert damping shows only a weak dependence on the external magnetic field in figure 5(b), the extrinsic damping, too, can be excluded [48]. In fact, the Gilbert damping parameter observed in our sample ($\alpha_{TRMO} \approx 2$–2.5×10^{-2}) is indeed rather large for a typical YIG and exceeds the value obtained from the room-temperature MW-FMR on the same sample by a factor of 5 ($\alpha_{FMR} \approx 1 \times 10^{-3}$, see supplementary material, section A). This seeming discrepancy can be explained by the temperature range in our TRMO experiment which was dictated by the increased noise level at elevated temperatures (see figure 4 in [49]). Significant increase in Gilbert damping (by a factor of 30) between room and low (20 K) temperature has been recently reported on a high quality YIG thin film [35] as well as on a bulk YIG [36], which was attributed to a presence of rare earth or Fe^{2+} impurities activated at cryogenic temperatures. The same effect can be expected in our YIG film, and is also consistent with the observed capping-dependent Gilbert damping shown in figure 5(b). The YIG/Pt structure is heated by the pump laser pulse to a higher temperature (see figures 5(c) and (d)) than the YIG/Au, which according to [35] corresponds to a lower Gilbert damping, as indeed observed experimentally.

It is worth noting that the damping parameter can be increased also by other mechanisms, as detailed in supplementary material, section D. Among them, the spin-pumping from YIG to the metallic layer is potentially the most interesting one. However, this effect is expected to be significantly higher when Pt is used as a the capping layer [50], which does not agree with our experimental results.

5. Conclusions

In conclusion, we demonstrated that magnetization precession can be induced in a plain thin YIG film by ultra-short, low peak power laser pulses, with a photon energy below the YIG absorption edge, if a thin metallic capping is deposited on the garnet layer. We stress that this method is quite universal—it could be applied for inducing a magnetization precession in any wide band gap magnetic insulator where laser sources for a resonant excitation of the material are not available. Based on the picosecond onsets in the measured signals, we identified triggering mechanism of the precession, which is clearly thermal and originates in the laser heating of the metal capping. As the heat propagates through the YIG layer towards the GGG substrate,

the resulting change of the sample temperature modifies its magnetocrystalline anisotropy, which sets the system out of equilibrium and initiates the magnetization precession. Based on the field dependence of precession frequency, we identify the induced magnetization dynamics as the fundamental (Kittel) FMR mode, which is virtually independent of the type of capping and reflects the quasi-equilibrium magnetic anisotropy of YIG. The TRMO experiment thus serves as an analogy to the standard MW-FMR while keeping the advantage of the all-optical approach in high spatial and temporal resolution. Furthermore, both the direction and the magnitude of the external magnetic field can be easily varied in the optical experiment, which enables to clearly extract intrinsic damping parameters [18]. Using this method, we identified that the Gilbert damping parameter was influenced by line-broadening mechanism due to low-temperature activation of impurities, which is an important aspect to be considered for low-temperature spintronic device applications.

When improving efficiency of the optical magnetization precession trigger, it was found that the type of metallic capping layer strongly influences the precession amplitude. The precession in YIG/Pt attained almost twice the amplitude of that in YIG/Au under the same conditions. This indicates that a suitable choice of a capping layer could help to optimize this local non-invasive magnetometric method, and make it suitable for further spintronic experiments, such as optical detection of spin-pumping or even ultrafast spin Seebeck effect.

Data availability statement

All data that support the findings of this study are included within the article (and any supplementary files).

Acknowledgments

This work was supported in part by the INTER-COST Grant No. LTC20026 and by the EU FET Open RIA Grant No. 766566. We also acknowledge CzechNanoLab project LM2018110 funded by MEYS CR for the financial support of the measurements at LNSM Research Infrastructure and the German Research Foundation (DFG SFB TRR173 Spin+X projects A01 and B02 #268565370).

ORCID iDs

Richard Schlitz https://orcid.org/0000-0001-5756-6716
Gerhard Jakob https://orcid.org/0000-0001-9466-0840

References

[1] Hirohata A, Yamada K, Nakatani Y, Prejbeanu I-L, Diény B, Pirro P and Hillebrands B 2020 *J. Magn. Magn. Mater.* **509** 16671
[2] Kirilyuk A, Kimel A V and Rasing T 2010 *Rev. Mod. Phys.* **82** 2731
[3] Siegrist F *et al* 2019 *Nature* **571** 240
[4] Němec P, Fiebig M, Kampfrath T and Kimel A V 2018 *Nat. Phys.* **14** 229
[5] Kimling J, Choi G M, Brangham J T, Matalla-Wagner T, Huebner T, Kuschel T, Yang F and Cahill D J 2017 *Phys. Rev. Lett.* **118** 057201
[6] Ortiz V H, Gomez M J, Liu Y, Aldosary M, Shi J and Wilson R B 2021 *Phys. Rev. Mater.* **5** 074401
[7] Malinowski G, Kuiper K C, Lavrijsen C, Swagten H J M and Koopmans B 2009 *Appl. Phys. Lett.* **96** 102501
[8] Gomez M J, Liu K, Lee J G and Wilson R B 2020 *Rev. Sci. Inst.* **91** 023905
[9] Tesařová N, Němec P, Rozkotová E, Šubrt J, Reichlová H, Butkovičová D, Trojánek F, Malý P, Novák V and Jungwirth T 2012 *Appl. Phys. Lett.* **100** 102403
[10] Wu G, Ren Y, Jin Q and Zhang Z 2020 *ACS Appl. Nano Mater.* **3** 11555
[11] Tang M, Li W, Ren Y, Zhang Z, Loub S and Jinab Q Y 2017 *RSC Adv.* **7** 5315
[12] Beaurepaire E, Merle J-C, Daunois A and Bigot J-Y 1996 *Phys. Rev. Lett.* **76** 4250
[13] Němec P *et al* 2012 *Nat. Phys.* **8** 411
[14] Choi G M, Schleife A and Cahill D G 2017 *Nat. Commun.* **8** 15085
[15] Tesařová N *et al* 2013 *Nat. Photon.* **7** 492
[16] Kimel A V, Kirilyuk A, Tsvetkov A, Pisarev R V and Rasing T 2004 *Nature* **429** 850
[17] Choi Y G and Choi G M 2021 *Appl. Phys. Lett.* **119** 022404
[18] Němec P *et al* 2013 *Nat. Commun.* **4** 1422
[19] Smith N G W, Pleimling Y, Magill B A, Mudiyanselage R R H H, Shenenberger S, Ogawa S, Nishizawa N, Munekata H and Khodaparast G A 2022 *J. Appl. Phys.* **132** 243902
[20] Ishibashi K, Iihama S, Takeuchi Y, Furuya K, Kanai S, Fukami S and Mizukami S 2020 *Appl. Phys. Lett.* **117** 122403
[21] Kats V N *et al* 2016 *Phys. Rev.* B **93** 214422
[22] Hashimoto Y, Kobayashi S and Munekata H 2008 *Phys. Rev. Lett.* **100** 067202
[23] Miwa S *et al* 2021 *Small Sci.* **1** 2000062
[24] Serga A A, Chumak A V and Hillebrands B 2010 *J. Phys. D: Appl. Phys.* **43** 264002
[25] Kajiwara Y *et al* 2010 *Nature* **464** 262
[26] Cherepanov V, Kolokolov I and L'vov V 1993 *Phys. Rep. Rev. Sec. Phys. Lett.* **229** 81

[27] Stancil D D and Prabhakar A 2009 *Spin Waves—Theory and Applications* (New York: Springer)
[28] Hansteen F, Kimel A, Kirilyuk A and Rasing T 2005 *Phys. Rev. Lett.* **95** 047402
[29] Stupakiewicz A, Pashkevich M, Maziewski A, Stognij A and Novitskii N 2012 *Appl. Phys. Lett.* **101** 262406
[30] Montazeri M *et al* 2015 *Nat. Commun.* **6** 8958
[31] Shelukhin L A, Pavlov V V, Usachev P A, Yu P, Shamray R, Pisarev R V and Kalashnikova A M 2018 *Phys. Rev.* B **97** 014422
[32] Stupakiewicz A, Szerenos K, Afanasiev D, Kirilyuk A and Kimel A V 2017 *Nature* **542** 71
[33] Atoneche F, Kalashnikova A M, Kimel A V, Stupakiewicz A, Maziewski A, Kirilyuk A and Rasing T 2010 *Phys. Rev.* B **81** 214440
[34] Schmoranzerová E *et al* 2022 *Phys. Rev.* B **106** 104434
[35] Jermain C L, Aradhya S V, Reynolds N D, Buhrman R A, Brangham J T, Page M R, Hammel P C, Yang F Y and Ralph D C 2017 *Phys. Rev.* B **95** 174411
[36] Maier-Flaig H, Klingler S, Dubs C, Surzhenko O, Gross R, Weiler M, Huebl H and Goennenwein S T B 2017 *Phys. Rev.* B **95** 214423
[37] Panda N S, Mondal S, Sinha J, Choudhury S and Barman A 2019 *Sci. Adv.* **5** 7200
[38] Gong Y *et al* 2021 *Appl. Phys. Lett.* **119** 092404
[39] Bhoi B, Kim B, Kim Y, Kim M-K, Lee J-H and Kim S-K 2018 *J. Appl. Phys.* **123** 203902
[40] Mendil J *et al* 2019 *Phys. Rev. Mater.* **3** 034403
[41] Lišková Jakubisová E, Višňovský Š, Chang H and Wu M 2016 *Appl. Phys. Lett.* **108** 082403
[42] Surýnek M, Saidl V, Kašpar Z, Novák V, Campion R P, Wadley P and Němec P 2020 *J. Appl. Phys.* **127** 233904
[43] We note that the FMR data were obtained at room temperature while the TRMO experiment was performed at 20 K. However, as apparent from figure 4(c), the precession frequency f varies by less than 10% between 20 K and 300 K, which is well below the experimental error of $f(\theta_H)$. This justifies comparison of the precession frequencies obtained from the TRMO experiment with the FMR data
[44] Janda T, Ostatnický T, Němec P, Schmoranzerová E, Campion R, Hills V, Šobáň Z and Wunderlich J 2022 *Sci. Rep.* **12** 21550
[45] Beaulieu N, Kervarec N, Thiery N, Klein O, Naletov V, Hurdequint H, de Loubens G, Youssef J B and Vukadinovic N 2018 *IEEE Magn. Lett.* **9** 3706005
[46] Lin H, Kou A, Cheng J, Dong H, Xu S, Zhang J and Luo S 2020 *Sci. Rep.* **10** 9165
[47] Zhang X, Xie H, Fujii M, Ago H, Takahashi K, Ikuta T, Abe H and Shimizu T 2005 *Appl. Phys. Lett.* **86** 171912
[48] Walowski J, Djordjevic Kaufmann M, Lenk B, Hamann C, McCord J and Münzenberg M 2008 *J. Phys. D: Appl. Phys.* **41** 164016
[49] Saidl V *et al* 2017 *Nat. Photon.* **11** 91–97
[50] Burrowes C and Heinrich B 2009 *Magnonics—From Fundamentals to Applications* vol 125 (New York: Springer) p 129